

# Performance Comparison of Fast, Transparent, and Biotic Heaters Based on Leaf Skeletons

Vipul Sharma,\* Katriina Jääskö, Kyriacos Yiannacou, Anastasia Koivikko, Vilma Lampinen, and Veikko Sariola\*

Bioinspired, highly flexible, fast, and biodegradable heaters are fabricated based on Ag nanowires and leaf skeletons of different plant species. The leaf skeletons act as transparent substrates with a high surface-area-to-volume ratio and allow a uniform dispersion of the Ag nanowires through the surface. Ag nanowires adhered to the leaf skeletons display very good transmittance (up to  $\approx 87\%$ ) and mechanical (flexibility) properties (curvature values  $> 800 \text{ m}^{-1}$ ) without any post-treatment. The flexible leaf skeleton-based heaters reach high temperatures very quickly, with very low voltages ( $< 4 \text{ V}$ ). The performance of the bioinspired heater surface is dependent on the types of fractal structures at the microscale. The morphology of the leaf skeletons is studied in detail and is correlated with the transmittance, flexibility, and sheet resistances. Bioinspired heater surfaces based on different leaf skeletons are compared based on their multiscale morphology, and the different heating performance parameters are screened. Based on the study conducted, insights on the best-performing biotic design for the fabrication of the heaters that are useful in practical wearable, medical, or industrial heating applications are provided.

## 1. Introduction


The advancement of the design and fabrication of transparent film heaters has gained attention in recent times due to their application in panel displays,<sup>[1]</sup> defrosters,<sup>[2]</sup> sensors,<sup>[3]</sup> and devices of industrial importance.<sup>[1,2,4]</sup> Currently, most of the reports in their design are directed toward wearable electronics, next-generation textiles, and flexible biomedical devices such as thermotherapy patches.<sup>[5–10]</sup> The thermotherapy patches improve blood circulation, stop inflammation, ease pain, and are very effective in the treatment of various types of arthritis.<sup>[11]</sup> For this application, optical transparency and portability, flexibility, fast response, breathability, and uniform heating are also important.<sup>[6,12]</sup> Various types

of conducting polymers,<sup>[4]</sup> semiconductor oxides,<sup>[13]</sup> their composites, and most recently carbon-based nanomaterials<sup>[14,15]</sup> have been proposed for flexible thermotherapy patches due to their flexibility, transparency, and good electrical conductivity. However, most of the heater surfaces are not very promising during different types of mechanical strains that occur during bending and folding. In addition, the surfaces require high voltages to reach the operating temperatures that limit their usage in thermotherapy patches.<sup>[1,3,7]</sup> In almost all the reports, the intrinsic and extrinsic mechanical and electrical properties of the materials take focus to improve the overall performance of the heater surfaces.

As an alternative, metallic nanowires have been developed to provide excellent transmittance and conductance and thus have been brought forward as a potential candidate for transparent electrical conductors

in thin-film flexible electronic devices.<sup>[16,17]</sup> In current times, the silver (Ag) nanowire network is the most explored conductive material for the fabrication of transparent electrodes and their applications due to its excellent conductivity, optical transparency in the visible region, and excellent flexibility.<sup>[18]</sup> However, an increase in the concentration of the Ag nanowires on the substrate decreases the sheet resistance and reduces the transmittance drastically.<sup>[19]</sup> This is because the increase in Ag nanowires concentration makes the layer thick, which hinders any light to pass through it. A random nanocrack network of Ag nanowires has been reported, where transparency of the surfaces can be maintained by bundling nanowires in a micro-mesh-like network.<sup>[20]</sup> Apart from Ag nanowires, Cu nanowires have been recently reported, which may provide a cost-effective alternative to Ag nanowires.<sup>[21–24]</sup> The arrangement of the nanowires in bundles or close contact with each other is also important for such applications. This is because metal nanowire-based networks sometimes display large junction resistance between nanowires and require annealing techniques such as regular thermal annealing, laser nanowelding, flash lamp welding, chemical-assisted joining, mechanical welding, etc.<sup>[25–29]</sup> The substrates used for these purposes are mostly polymers such as polyethylene naphthalate, polyethylene terephthalate, polyimide, etc.<sup>[1,3,4,30,31]</sup> These polymers have high thermal resistance that leads to low thermal efficiency, slow thermal response, and high input voltages. Apart from engineering the intrinsic properties of the material, the architecture of the films at the micro- and

V. Sharma, K. Jääskö, K. Yiannacou, A. Koivikko, V. Lampinen, V. Sariola  
Faculty of Medicine and Health Technology  
Tampere University  
Korkeakoulunkatu 3, 33720 Tampere, Finland  
E-mail: vipul.sharma@tuni.fi; veikko.sariola@tuni.fi

 The ORCID identification number(s) for the author(s) of this article can be found under <https://doi.org/10.1002/adem.202101625>.

© 2022 The Authors. Advanced Engineering Materials published by Wiley-VCH GmbH. This is an open access article under the terms of the Creative Commons Attribution License, which permits use, distribution and reproduction in any medium, provided the original work is properly cited.

DOI: 10.1002/adem.202101625

nanoscale also plays an important role in maximizing the efficiency of the Ag nanowires-based film heaters.<sup>[6]</sup>

Bioinspired surfaces with special functionalities have grabbed attention in engineering research in recent times. The microstructures and mechanisms behind these functional biological surfaces with interesting properties have inspired scientists to engineer functional devices that integrate biotic designs and material properties along with traditional fabrication methodologies. Among bioinspired architectures, fractals are structures that appear similar at all length scales and fractal-like structures can be found in nature in abundance. Fractal-like structures can be seen at many places, for example, snowflakes and leaf venations, and display structures on multiple length scales. Fractal designs that provide the high surface coverage, improved stability, and efficient transport of ions have been reported.<sup>[32]</sup> Fractal designs also facilitate the efficient collection of electrical and thermal energy and therefore these have been used in different applications such as photovoltaics, sensors, etc.<sup>[33–35]</sup> Fractal-based designs are also advantageous in the field of flexible electronics as this overcomes the limitations of the conventional planar designs by maximizing the surface area at the microscale or, more specifically, maximizing the surface-area-to-volume ratio via simple scaling.

Bioinspired surfaces can serve as guides to engineer the surfaces to improve the heating efficiency of the thin-film heaters. In our previous work, we demonstrated that the leaf skeletons of *Ficus religiosa* can be used as the substrates to hold the Ag nanowires to achieve good heating performances with the rapid heating and cooling rates, that was due to the low thermal mass of the leaf skeleton and the high surface area of the fractal-like geometry.<sup>[6]</sup> However, the study was limited to fractal structures of just one leaf skeleton. As leaf skeletons based on different plant species offer unique fractal architecture, our previous study did not answer the question of how well the results generalize to other plant species and how the architecture of different plant species influences the performance of flexible heaters. In this study, we fabricated bioinspired, highly flexible, and transparent heaters based on fractal-like leaf skeletons belonging to different plant species (*Populus tremuloides*, *Bauhinia blakeana*, *Ficus macrocarpa*, *Ligustrum lucidum*, *Magnolia sieboldii*, *Epipremnum aureum*, *Quercus velutina*, and *Hevea brasiliensis*) and compared their performances. Different leaf skeletons were chosen based on their availability and visible transparency. A simple drop-cast method was utilized to load the Ag nanowires (in water) onto the leaf skeletons. The presence of the microstructures and porous architecture soaks the water and allows the nanowires to form a network across the skeleton surfaces (Video V1, supporting information). Depending on the type and the orientation of the fractal structures, the fabricated electrodes displayed different electrical and optical properties. Various properties of the fabricated surfaces were correlated with the heating performance and the overall efficiencies were evaluated. The insights from this study may help to screen fractal-like structures from nature that can be used for different domains of flexible electronics.

## 2. Results and Discussions

The fabrication procedure of the leaf skeleton-based conducting surfaces is described in the Experimental Section and

schematically illustrated in **Figure 1a**. To fabricate the bioinspired heaters, the leaves belonging to different plant species were chosen based on their different shapes and visible transparency. A necessary prerequisite for selecting a species was that one should be able to skeletonize its leaves. All the skeletons show fractal-like interconnections of veins that range from micro- to milliscale. In the first step, the leaf skeletons were cut into suitable pieces and mounted on a plastic frame. Then, small drops of Ag nanowires (in water) were placed on the leaf skeletons and spread evenly throughout the surface. The surface was left to dry until the solution was completely evaporated or soaked by the skeleton, leading to attachment of the Ag nanowire network onto the surfaces. High-aspect-ratio Ag nanowires were used to minimize the junction resistance and decrease the intrinsic resistance.<sup>[36]</sup> The orientation of the fractals also might affect the assembly of Ag nanowires. This might lead to the increase or decrease in the junction resistance even when the loading amount of the Ag nanowires is the same and this would result in the variation in sheet resistances. The details of the fabrication process are provided in the Experimental Section (supporting information).

Variations in the leaf orientations and the shapes are because of the adaptations of different plant species according to various factors.<sup>[37]</sup> The architecture and the mechanical properties of the leaf skeletons derived from these leaves also vary. **Figure 1b** shows the leaf skeletons of different plant species which are used in this study. From the images, it is apparent that shapes, sizes, and transparencies are visibly different when compared with each other. If the surfaces are to be applied in the applications such as thermotherapy patches or electronic skins, transparency is an important parameter that allows the precise monitoring of the healing process and biosignals.<sup>[38]</sup> We have previously demonstrated that there is no significant change in the transmittance values when the concentration of Ag nanowires deposited on the skeleton surfaces changes as the deposition takes place at the leaf veins and there are many holes on the surface. Usually, on the conventional polymer-based substrates, an increase in Ag nanowire loading sacrifices the transparency because of the rise in the reflection of photons and stronger scattering. In our previous studies, we have demonstrated that the conductivity of Ag nanowires-coated leaf skeletons depends on the Ag nanowires loading concentration without any significant change in the transmittance.<sup>[6,39]</sup> To compare the transparency of the bioinspired heater electrodes based on different leaf skeletons, we measured the optical transmittance spectra of the leaf skeletons loaded with fixed concentrations ( $\approx 160 \mu\text{g cm}^{-2}$ ). **Figure 1b** shows the camera images of the different leaf skeletons displaying the visible difference in the transparencies. **Figure 1c** shows that the different leaf skeletons allow light to pass through them between the visible and near-infrared regions (400–900 nm). It is evident from **Figure 2c** that the transmittance values of the leaf skeletons vary from  $\approx 40\%$  to  $\approx 87\%$ . Out of all the leaves, *Magnolia sieboldii* shows the best transparency ( $\approx 87\%$ ) closely followed by *Populus tremuloides* ( $\approx 84\%$ ). Leaf skeletons of *H. brasiliensis*, *Ligustrum lucidum*, *E. aureum*, and *Bauhinia blakeana* show transparency in the range of 55–74% that is typical for most leaf skeletons. Leaf skeletons of *Quercus velutina* and *Ficus microcarpa* showed the lowest transparency ( $\approx 40\%$ ), which is also evident from the camera images in addition to the transmittance spectra. As expected, Ag nanowire loading did not significantly affect the transmittance values of the leaf

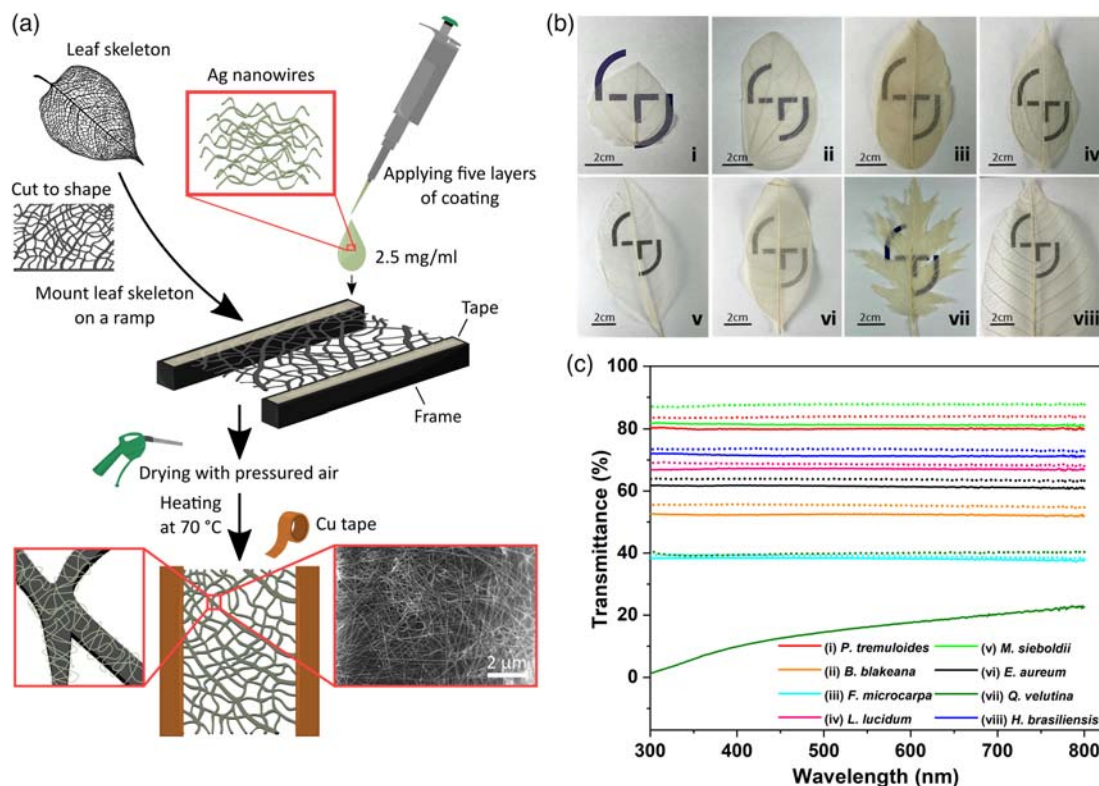


**Figure 1.** a) Schematic of the fabrication procedure. b) Camera images of the different leaf skeleton surfaces: i) *P. tremuloides*, ii) *B. blakeana*, iii) *F. microcarpa*, iv) *L. lucidum*, versus v) *M. sieboldii*, vi) *E. aureum*, vii) *Q. velutina*, and viii) *H. brasiliensis*. c) Transmittance values of the Ag-loaded ( $\approx 160 \mu\text{g cm}^{-2}$ ) leaf skeletons of different plants species. Solid lines in (c) represent the Ag nanowires-loaded surfaces and dotted lines show the bare (no Ag loading) surfaces.

skeletons and, barring *Q. velutina*, the Ag-coated leaf skeletons only displayed 6 percentage points or less decrease in the overall values (Figure 1c).

The scanning electron micrographs of the leaf skeletons coated with Ag nanowires are shown in Figure 2. The images clearly show that there is an architectural difference between the fractal structures of different leaf skeletons. Figure S1, Supporting Information, shows further magnified scanning electron microscope (SEM) images that show the significant difference in the bundles of vessels and interconnected fibers. Cell blocks in some of the skeletons are short, as evident from Figure S1, Supporting Information, while some show the long continuous bundles, as summarized in Table 1. The fractals of the different leaf skeletons have different arrangements of fiber interconnections and the distances range from a few micrometers to a few hundred micrometers. The distances are calculated based on the SEM images and are summarized in Table 1. Figure S2, Supporting Information, shows the arrangement of the Ag nanowires after they adhered to the leaf skeletons. The Ag nanowires used in the study have an average aspect ratio of  $\approx 1000$  and, as evident from the SEM images, the nanowires uniformly adhere to the surface. There are numerous micropores on the skeletons that soak the Ag nanowire dispersion liquid (water), leaving nanowires on the surface (Video V1, Supporting Information). The arrangement of the nanowires shows a continuous network that spreads across the leaf skeleton surface.

The optical, mechanical, and heating properties depend on the morphology of the fractals at the microscale. To investigate the fractal orientation and the fractal morphology, the total area covered by the skeletons was also calculated using ImageJ software. From the data, *Q. velutina* and *E. aureum* had the maximum area coverage with  $\approx 89 \pm 4\%$  and  $\approx 63 \pm 12\%$ , respectively. As shown in Figure 3a, most of the leaf skeletons had average surface coverage in the range of 40–60%. The skeletons of *M. sieboldii* had the lowest average surface coverage of  $\approx 39 \pm 10\%$  with some samples even showing coverage of  $\approx 35\%$ . The skeletons based on *L. lucidum* also had low area coverage with some samples showing the fractal coverage of  $\approx 39\%$ . However, the network, in this case, was not as dense as observed in the other skeletons. The values obtained from the surface area coverage also correlate well with the transmittance values, as shown in Figure 1b,c. Hence, lesser surface area coverage tends to increase the transparency of the leaf skeletons.

Fractal analysis is generally used to describe the complexity of plant structures. Fractal dimension is a value that can account for how a fractal pattern changes with the scale at which it is measured. It can be also used to measure how a fractal pattern scales differently from the topological space it is embedded and can be used to complement the area coverage or space filling of the microstructures.<sup>[40]</sup> To further gain insight regarding the surface morphology of the leaf skeletons, dimensions of the fractals (FD) were calculated using the box-counting method in



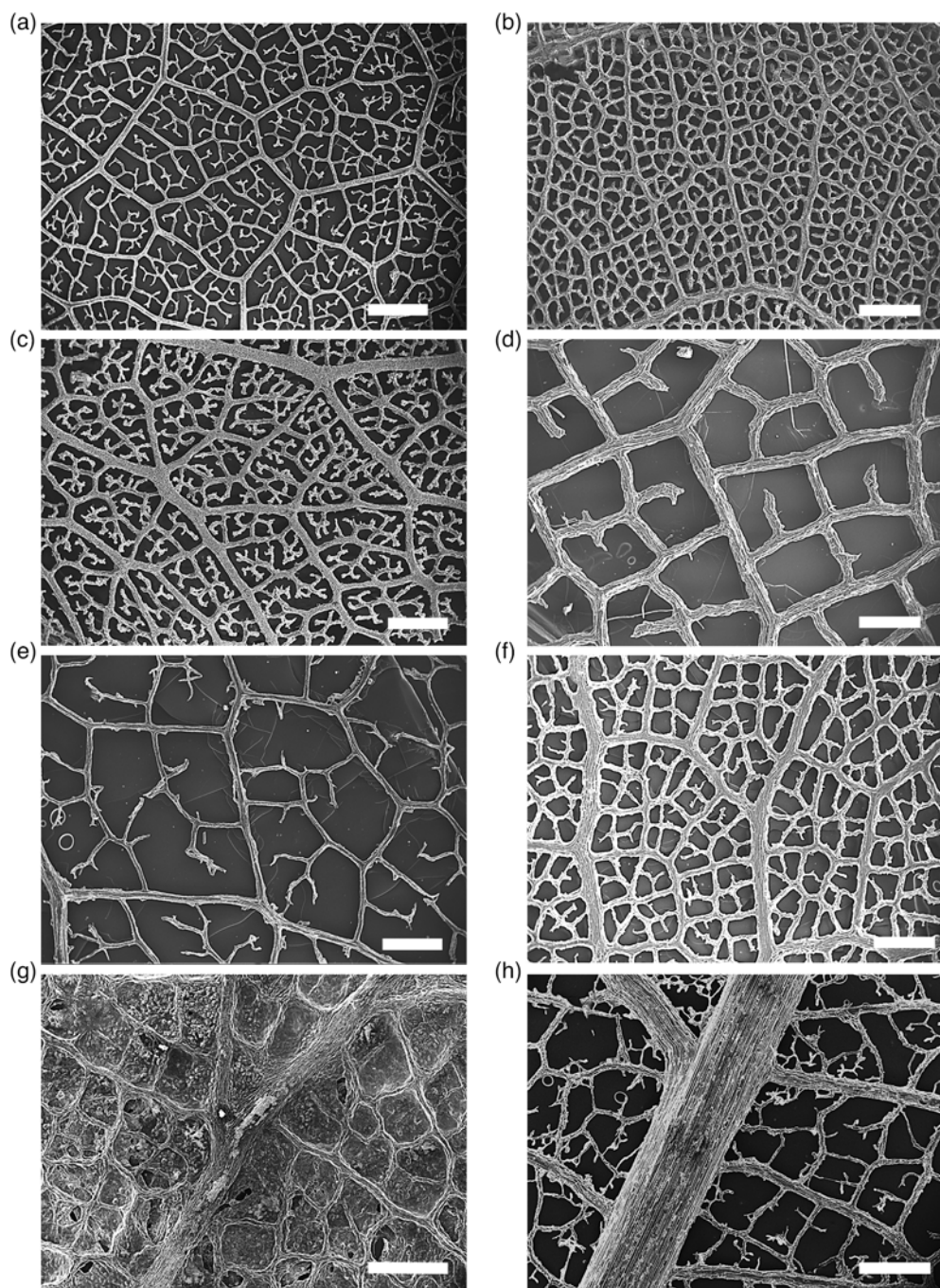


**Figure 2.** SEM images of a) *P. tremuloides*, b) *B. blakeana*, c) *F. microcarpa*, d) *L. lucidum*, e) *M. sieboldii*, f) *E. aureum*, g) *Q. velutina*, and h) *H. brasiliensis* plant-based leaf skeletons. Scale bars: 500  $\mu\text{m}$ .

ImageJ.<sup>[41]</sup> The results of the fractal dimension calculations for the leaf skeletons are summarized in Table 1. As evident from the data, the FD of almost all the leaf skeletons ranged between 1.5 and 1.8, which is typical for the leaf skeletons reported in the literature.<sup>[42,43]</sup> The skeletons based on *B. blakeana* showed the highest FD value of  $1.721 \pm 0.001$  followed by *F. microcarpa* ( $1.718 \pm 0.01$ ) and *E. aureum* ( $1.708 \pm 0.001$ ). The values also correspond well with the SEM images that show a very dense

network of fractals. As expected, the skeletons of *M. sieboldii* ( $1.589 \pm 0.013$ ) had FD in a slightly lower range that is also in agreement with the SEM data where a less dense network is evident.

To compare the effect of the fractal architecture on the conductivity, we loaded  $\approx 160 \mu\text{g cm}^{-2}$  Ag nanowires onto the surface using the procedure detailed in the Experimental Section. This loading concentration of the nanowires was kept the same

**Table 1.** Morphology observations of leaf skeletons.

S.No.	Leaf skeleton	Fiber interconnection gap [ $\mu\text{m}$ ]	Cell blocks [length in $\mu\text{m}$ ]	Fractal dimensions [FD]
1	<i>P. tremuloides</i>	$\approx 80\text{--}100$	Short ( $\approx 5\text{--}15$ )	$1.681 \pm 0.001$
2	<i>B. blakeana</i>	$\approx 50$	Short ( $\approx 5\text{--}15$ )	$1.721 \pm 0.001$
3	<i>F. microcarpa</i>	$\approx 20\text{--}30$	Short ( $\approx 5\text{--}20$ )	$1.718 \pm 0.01$
4	<i>L. lucidum</i>	$\approx 200\text{--}500$	Long ( $>90$ )	$1.631 \pm 0.002$
5	<i>M. sieboldii</i>	$\approx 100\text{--}300$	Long ( $>50$ )	$1.589 \pm 0.013$
6	<i>E. aureum</i>	$\approx 50\text{--}100$	Medium–Long ( $\approx 20\text{--}100$ )	$1.708 \pm 0.001$
7	<i>Q. velutina</i>	–	–	–
8	<i>H. brasiliensis</i>	$\approx 50\text{--}200$	Short ( $\approx 5\text{--}50$ )	$1.674 \pm 0.029$

in all the samples and sheet resistance was measured. Except for *Q. velutina*, all the skeleton-based electrodes displayed uniform sheet resistance values that were less than  $10 \Omega \text{sq}^{-1}$ , as shown in the inset of Figure 3b. Conductive leaf skeletons based on *Q.*

*velutina* displayed comparatively higher resistances  $> 50 \Omega \text{sq}^{-1}$  that could be because of a very limited gap between the interconnected fibers and more area coverage (refer to Figure 2). This arrangement would require a greater number of nanowires that usually is reported in the planar thin-film heater surfaces. The fractal structures having thinner fractal dimensions ( $<100 \mu\text{m}$ ) and area coverage less than  $\approx 60\%$  displayed the average sheet resistance lesser than  $10 \Omega \text{sq}^{-1}$ . The surfaces based on *P. tremuloides* displayed the lowest sheet resistance. However, if the area coverage and corresponding resistances are taken into consideration, *M. sieboldii*-based surfaces displayed the lowest sheet resistances and area coverage, as shown in Figure 3b.

To gain further insight into how the different leaves compare in terms of their conductivity and transparency, we calculated two different figures of merit (FOM) for the different leaves using equations

$$\Phi_{\text{TC}} = \frac{T^n}{R_S} \quad (1)$$

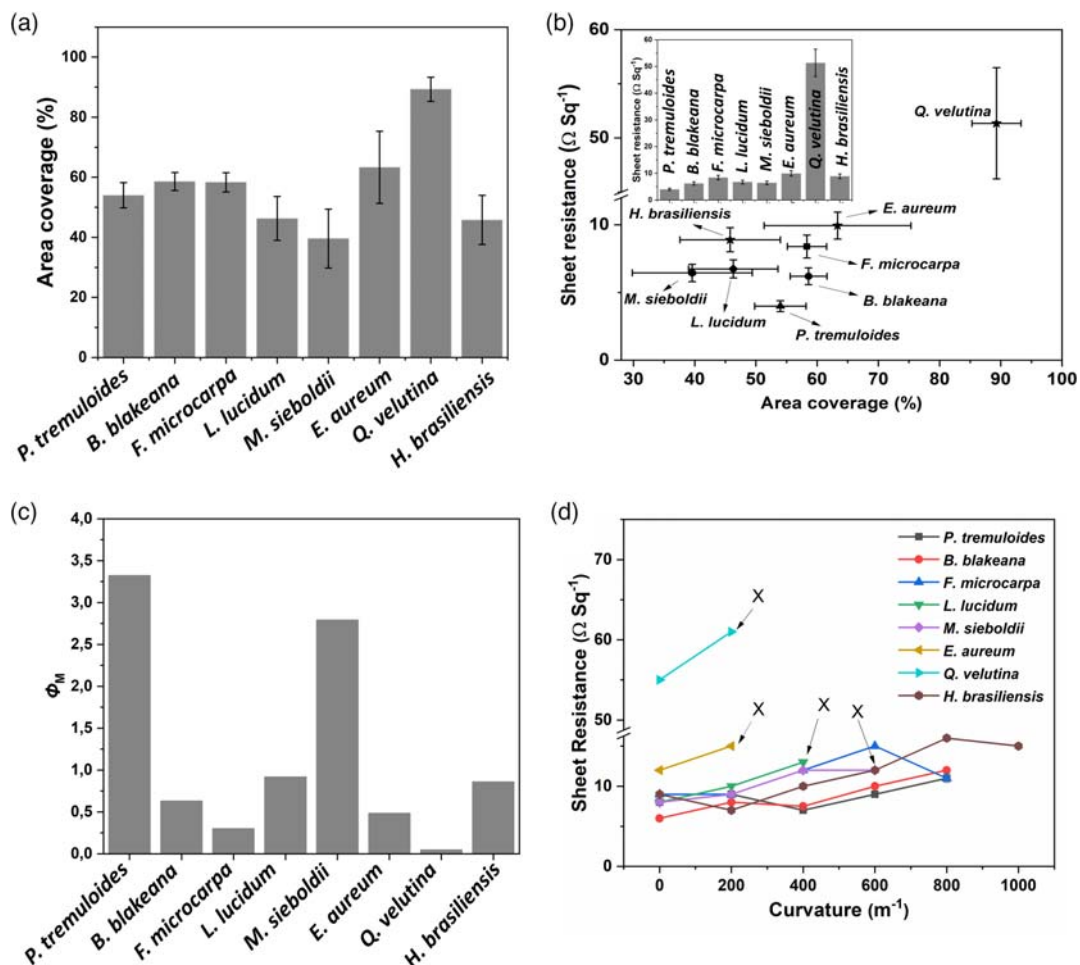


**Figure 3.** Conducting surfaces characterization: a) percentage (%) area covered by the fractals and b) sheet resistance of the different skeleton surfaces with fixed Ag nanowires loading ( $\approx 160 \mu\text{g cm}^{-2}$ ) plotted against the area coverage. The inset shows the sheet resistance corresponding to different Ag nanowire-covered leaf skeletons. c) FOM ( $\Phi_M$ ) values corresponding to different leaf skeletons d) show the resistance values of different Ag-loaded leaf skeletons plotted against their corresponding curvatures.

$$\Phi_M = -\frac{1}{R_s \log T} \quad (2)$$

where  $T$  is the average transmittance value in the visible range,  $R_s$  is the sheet resistance, and  $n$  is a parameter that adjusts how the FOM weighs transmittance relative to sheet resistance in Equation (1).<sup>[44]</sup> Equation (1) was proposed by Haacke,<sup>[44]</sup> who studied how the FOM ranks different surfaces when  $n = 1$  or  $n = 10$ ; here, we used  $n = 10$ . We derived  $\Phi_M$  (eq. 2) from  $\Phi_{TC}$  (Equation (1)) using the following reasoning: for surfaces that follow Beer–Lamberts law

$$T = \exp(-\alpha t) \quad (3)$$

where  $\alpha$  is the optical absorption coefficient and  $t$  is the thickness.<sup>[44]</sup> At the same time, the sheet resistance

$$R_s = \rho/t \quad (4)$$

where  $\rho$  is the electrical resistivity of the material. Even if leaf surfaces cannot be thinned beyond their normal thickness, many layers of leaves can be stacked on top of each other, giving  $\tilde{T} = T^k$  or  $k = \log(\tilde{T})/\log(T)$ , and  $\tilde{R}_s = R_s/k$ , where  $\tilde{T}$  and  $\tilde{R}_s$  are the transmittance and sheet resistance after stacking multiple samples on top of each other. If for every sample enough layers would be stacked until they have the same transmittance  $\tilde{T}$ , then

$\Phi_{TC} = \frac{\tilde{T}^n}{R_s} = \frac{\tilde{T}^n}{R_s \log(\tilde{T})/\log(T)} \sim -\frac{1}{R_s \log T} = \Phi_M$ , given that  $\tilde{T}$  was the same for all stacks of leaves. The minus sign was kept having larger values, indicating better surfaces for both FOM. To summarize,  $\Phi_M$  ranks the surfaces the same as  $\Phi_{TC}$ , provided that the thickness of each sample is adjusted so that each sample has the same transmittance. Furthermore, plugging in (3) and (4) into (2), we have

$$\Phi_M = \frac{1}{\rho\alpha} \quad (5)$$

which further shows that  $\Phi_M$  is independent of the thickness and only dependent on the intrinsic material properties.

The calculated results based on the new FOM are given in Figure 3c. The heater surfaces based on *P. tremuloides* with Ag loading of  $\approx 160 \mu\text{g cm}^{-2}$  had the best  $\Phi_M$  value of  $3.324 \Omega^{-1}$  ( $T = \approx 84\%$ ,  $R_s = \approx 4 \Omega \text{ sq}^{-1}$ ), representing good agreement between  $R_s$  and  $T$ . Heater surfaces based on *M. sieboldii* closely followed with  $\Phi_M$  value of  $2.792 \Omega^{-1}$  ( $T = \approx 88\%$ ,  $R_s = \approx 6.4 \Omega \text{ sq}^{-1}$ ). Such conducting surfaces applied for the transparent heater are expected to meet the requirements of maintaining visually high transmittance and low reflectance not only when used as thermotherapy patches, but also for other applications. The new FOM values calculated also correspond well to the ones proposed by Haacke,<sup>[44]</sup> where heater surfaces based on *P. tremuloides* and *M. sieboldii* show the highest FOM values of  $\Phi_{TC} = 0.0442$  and  $0.0432 \Omega^{-1}$ , respectively (Figure S3, Supporting Information).

If the conducting surfaces are to be used in flexible electronics applications, these should be flexible, without plastic deformation or cracking. To compare the flexibility of the different leaf skeletons, the surfaces were clamped from their edges

and bent with the help of a linear translation stage. The curvature of the leaf and the resistance of the electrodes were recorded during this process and the results are shown in Figure 3d. The plot also shows the maximum curvature values until the leaves were snapped. As expected, the resistances of the surfaces did not change much and that can be credited to the high aspect ratio and conformal attachment of the Ag nanowires. However, as evident in the figure, there was a significant difference in the maximum curvature values of the leaf skeletons of different species. The leaf skeletons based on *P. tremuloides*, *B. blakeana*, *F. macrocarpa*, and *H. brasiliensis* displayed the best flexibilities with curvature values exceeding  $800 \text{ m}^{-1}$ . *E. aureum* and *Q. velutina* displayed the least flexibility, and the electrodes based on them snapped around the curvature of  $200 \text{ m}^{-1}$ . Electrodes based on *L. lucidum* and *M. sieboldii* had slightly better flexibility, but the electrodes snapped before the curvature values of 400 and  $600 \text{ m}^{-1}$ . As the leaf skeletons are made up of organic matter based on lignin, the difference in the flexibility can be correlated with the arrangement of the microstructures. Based on the SEM images displayed in Figure 2 and the curvature values, we observed that the skeletons that have small blocks of cells in their fractals are more flexible. The cell blocks with a longer orientation are more prone to snapping at the lower-curvature values.

When the Ag nanowire-coated leaf skeletons are used as heaters, various performance parameters are to be considered that are required in specific applications. Apart from the mechanical and optical parameters, other parameters include low operating voltages, fast response times, uniform heating across the surface, steady temperature, and good heating rates. The Joule heating characteristics of different leaf skeletons were studied for the  $\approx 160 \mu\text{g cm}^{-2}$  Ag nanowire density. For this, a continuous DC voltage was applied between the two edges of the heater having dimensions of  $2 \text{ cm} \times 2 \text{ cm}$  and the heating properties were evaluated (details in the Experimental Section). Figure 4 shows the infrared images of the different leaf skeletons bearing a network of Ag nanowires when a bias of 2 V was applied. As evident from the images, almost all the skeleton-based electrodes show a rise in temperature throughout the surface. The infrared images shown in Figure 4 illustrate the uniformity of heating across the surfaces. This is also the indicator of the uniform distribution of the Ag nanowires across the surface. Upon comparison, the heater surfaces based on *H. brasiliensis* showed the most uniform heating throughout the surfaces even when bent (refer to Figure S4, Supporting Information). The electrodes based on *M. sieboldii* and *B. blakeana* also showed uniform heating on the surface that may be credited to the uniform distribution of the nanowires. The heaters based on *E. aureum* skeletons showed slightly uneven heat distribution. This may be due to the presence of uneven microstructures that are composed of medium–long cell blocks and might be responsible for uneven heat transfer. In addition, the skeleton-based heater surfaces are stable as well. A tape test was conducted on the heater surfaces based on *H. brasiliensis* as it showed most uniform heating (Figure S5, Supporting Information). A scotch tape (3M) was applied to the heater surface, pressed with a finger, and then peeled off after 5 s. Uniform heating on the surface was observed even after tape removal. The electrical tape (3M) was applied to the same surface and the process was repeated. The heater



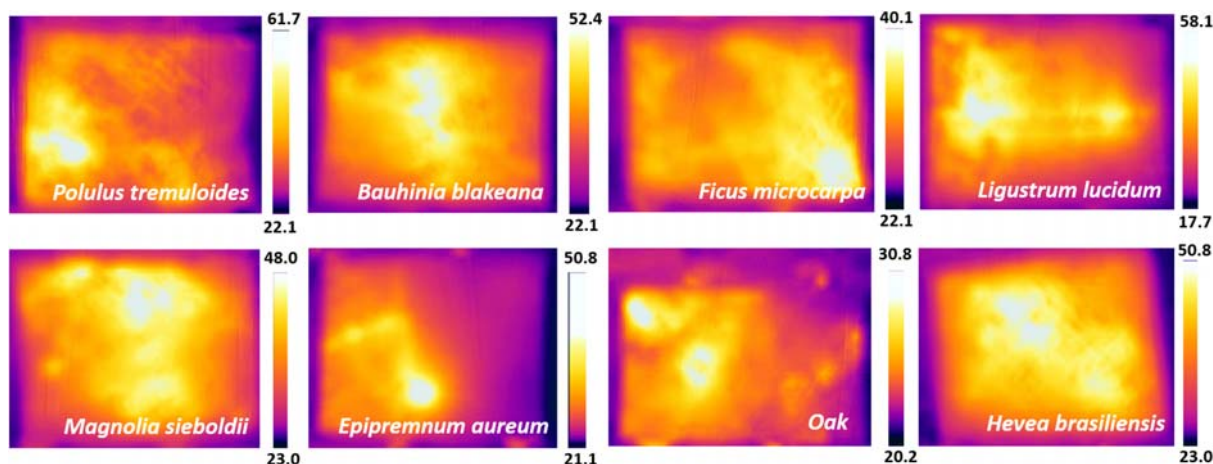


**Figure 4.** Infrared camera images of the bioinspired heater surfaces based on different leaf skeletons. The Ag nanowire loading is  $160 \mu\text{g cm}^{-2}$  and the bias applied is 2 V.

surface was able to maintain uniform heating, proving that the Ag nanowires are still present on the surface and the surface is stable.

To compare the heating characteristics, the heater surfaces were subjected to different bias voltages (1 V increment) and the temperature was recorded until the heater failed (Figure 5a). The electrodes based on *F. macrocarpa* and *M. sieboldii* recorded average highest temperatures of  $\approx 130^\circ\text{C}$  (3 V) and  $\approx 139^\circ\text{C}$  (4 V), respectively, before failure. The electrodes based on *B. blakeana* (up to  $\approx 128^\circ\text{C}$  at 4 V) and *H. brasiliensis* (up to  $\approx 120^\circ\text{C}$  at 4 V) also displayed high temperatures with steady temperature increases. The heater surfaces based on *Q. velutina* and *E. aureum* displayed the lowest range of temperatures (max temperatures  $\approx 55^\circ\text{C}$  at 8 V and  $\approx 72^\circ\text{C}$  at 2 V). It is noteworthy to mention that with decreased loading of the Ag nanowires, the temperature ranges can be controlled, and the surfaces are stable for higher voltages as well.<sup>[6]</sup> The heater surfaces fail at various voltages and this may be due to very high local temperatures at some points, which may result in the breakage of the Ag nanowires.<sup>[19,45]</sup>

To compare the response time and reliability of the heater surfaces, their time-dependent temperature profiles were recorded. Figure 5b displays the time-dependent temperature profiles of heaters belonging to different leaf skeletons. For each heater, the Ag nanowire loading was kept fixed, and the temperature was recorded at 2 V. From the figure, the temperature increased almost instantaneously in all the heater surfaces and reached their corresponding operating temperatures within  $\approx 15$  s. From the figure, it is also clear that almost all the skeleton-based heaters can maintain a steady-state temperature until the voltage is turned off. Rapid cooling was also observed in all the skeleton surfaces with the temperatures dropping immediately as soon as the voltage is turned off. For measurements of individual skeletons, three independent heater samples having the same Ag nanowire loading were tested at the same bias of 2 V, and the average values were taken into the consideration. However, the age, size, and shape of the leaf can lead to a slight variation in the orientation of the

microstructures. This may also cause greater variations in the performance of the heater as well. Ag nanowires and leaf skeleton-based heaters show extremely fast response times, and this is one of the main virtues of transparent heater surfaces. This is because of the fast heat exchange, as reported in the study by Sharma et al.<sup>[6]</sup> Figure 5c shows the time taken by each heater surface to reach operating temperature. From the values, the skeletons based on *E. aureum* and *F. macrocarpa* were the fastest to reach the operating temperatures ( $\approx 4.5$  and 5.5 s, respectively). Although almost all the heaters were very fast with most of the surfaces reaching the operating temperatures in less than 9 s. In comparison, only heaters based on *M. sieboldii* ( $\approx 11$  s) and *B. blakeana* ( $\approx 14$  s) took slightly more time to reach the operating temperatures. Based on the time taken to reach the operating temperatures, the rate constants for the heater surfaces were also calculated. Based on the data, the heaters based on *P. tremuloides* and *E. aureum* displayed the best rate constants with the average values of  $\approx 4.4$  and  $\approx 4.5^\circ\text{C s}^{-1}$ , respectively. Skeletons based on *H. brasiliensis* also had very good heating rates with an average value of  $\approx 3.7^\circ\text{C s}^{-1}$ . In comparison, heaters based on *Q. velutina* skeletons displayed the lowest rate constant of  $\approx 0.5^\circ\text{C s}^{-1}$ .

Almost all the heater surfaces belonging to the leaf skeletons of different plant species displayed first-order dynamics and had very rapid heating and cooling. As expected, the heat transfer was directly related to the applied voltages, that is, higher voltages corresponding to higher temperatures. Like reported previously, the good heating profile and the quick response times are due to the lower thermal mass of the leaf skeletons (mostly composed of a porous network of the lignin and cellulose) in addition to the very high surface area provided by the fractal-like geometry.

There are three forms of heat transfer, convection, conduction, and radiation, and their energy balance can be expressed by

$$Q_{\text{total}} = Q_{\text{conduction}} + Q_{\text{convection}} + Q_{\text{radiation}} \quad (6)$$

where  $Q_{\text{total}}$  is the generated heat;  $Q_{\text{conduction}}$  is the heat by thermal conduction, which can be neglected because the conduction losses are caused by external parts of the system;<sup>[3]</sup>  $Q_{\text{convection}}$

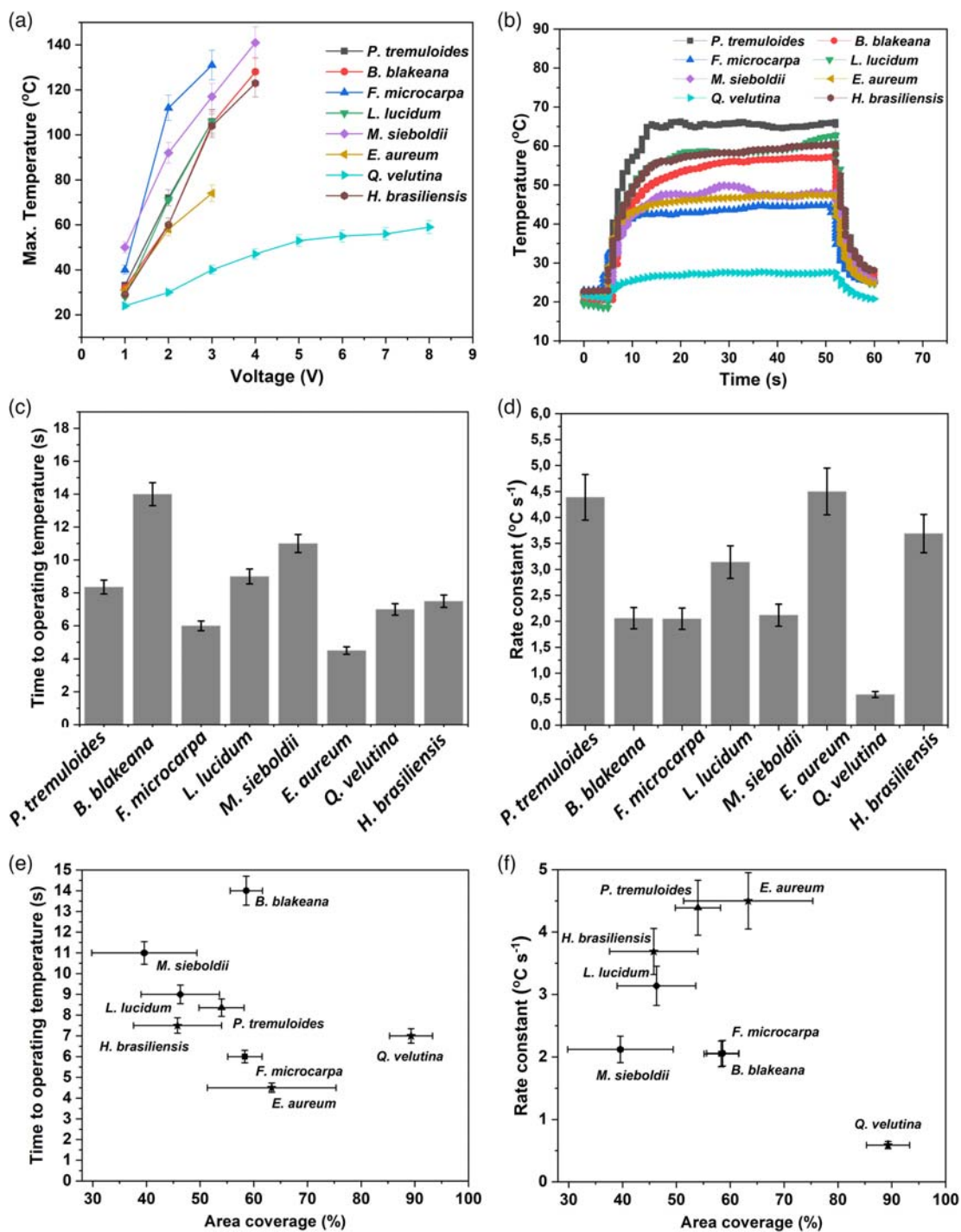


**Figure 5.** a) Highest temperature of the bioinspired heater surfaces when the voltages are increased in 1V increment until the heater fails. The Ag nanowires loading is  $\approx 160 \mu\text{g cm}^{-2}$  on all the surfaces. b) Time-dependent surface temperatures of the heater surface having different fractal surfaces and same Ag nanowires loading ( $\approx 160 \mu\text{g cm}^{-2}$  at 2 V). c) Time taken (s) by each heater surface to reach the operating voltage at 2 V and d) calculated rate constants of the surface to reach the operating temperature at 2 V. The error bars show the standard deviations calculated from three independent measurements. e,f) The relationship between the surface coverage to response times and rate constants, respectively.



is the convective heat loss in air; and  $Q_{\text{radiation}}$  is the radiative heat loss. As reported in the literature,  $Q_{\text{radiation}}$  is applicable only for high temperatures.<sup>[12,46]</sup> This is because the radiative heat transfer coefficient of Ag with the lowest emissivity is small compared with the overall heat transfer coefficient. Hence, the heat in the skeleton-based heaters is mainly generated by convective heat in the air and the conductive heat when the power ( $P$ ) is supplied to the surfaces based on Joule's law.

$$P = \frac{U^2}{R} = c\rho V \frac{dT}{dt} + hA(T - T_0) \quad (7)$$

where  $c$  is specific heat capacity,  $\rho$  is the density,  $V$  is the volume of the surface,  $h$  is the heat transfer coefficient,  $A$  is the surface area,  $T$  is the surface temperature of the electrical heater, and  $T_0$  is the temperature of the environment. Equation (7) is a first-order linear differential equation and has a time constant  $\tau = \frac{c\rho V}{hA}$ . Assuming that  $c$ ,  $\rho$ , and  $h$  are approximately constants, the response time of the heater can be made faster simply by increasing its surface-to-volume ratio. Also, the steady-state temperature is given by

$$T_{t \rightarrow \infty} = \frac{U^2}{RhA} + T_0 \quad (8)$$

This means that an increase in the steady-state temperature and the heating power is proportional to the surface area, and this avoids the overheating of the heating element. Hence, the high surface area-to-volume ratio plays an important role in heating performance. Different leaf skeletons have different fractal structures and hence varying surface-to-volume ratios. Surface area coverages (refer to Figure 3a) serve as indicators that how much volume the fractals have covered. Lesser coverage means that the density of the Ag nanowires will be increased per unit area, leading to a decrease in the resistance. More surface coverage means that the surface-to-volume ratio is compromised that will have an impact on the response times and the temperature range. Although most of the leaf skeletons provide good surface coverage, high surface area, and minimum in-plane resistance, it would be worth predicting the best coverage range while designing devices.<sup>[35,47]</sup> Figure 5e,f shows the relationship between the surface coverage to response times and rate constants, respectively. The heater surfaces based on *E. aureum* (surface coverage =  $\approx 63 \pm 12\%$ ) displayed the best performance in terms of response times and rate constants. Based on the data displayed in Figure 5e,f, it is safe to say that the good surface coverage range to design the heater is  $\approx 45\text{--}63\%$ . It is noteworthy to mention that the FD does not seem to have a direct impact on the heating characteristics of the surfaces.

Overall, the results reveal that the architecture of the leaf skeletons has a significant influence on the optical, mechanical, electrical, and thermal characteristics of Ag nanowires-coated leaf skeletons. The orientation and the arrangement of the structural lignin influence the flexibility and give insight toward the flexible surfaces. Surface area coverage, the gap between the fractals, and the fractal dimensions are also important parameters that influence the heating performances. Heater surfaces based on various skeletons excel at many individual parameters such as high optical transparency, high flexibility, stable and high

operating temperatures, and very rapid response times. Based on the analysis, the heater surfaces based on *H. brasiliensis* performed well and displayed good transparency, flexibility, uniform heating, stable operating temperatures complemented by the rapid response times, and good rate constants.

### 3. Conclusion

In pursuit of an ideal biotic design for the fabrication of the heating patches for thermotherapy, we fabricated the heater surfaces based on leaf skeletons of different plant species. Ag nanowires were coated onto the skeleton surfaces to obtain heater surfaces. The optical transmittance, flexibility, and heating properties were studied in detail and were correlated with fractal architectures at the microscale. Based on the performance analysis, we conclude that the leaf skeletons based on *H. brasiliensis* provide overall a good substrate for fabricating heaters that could be directly utilized in thermotherapy applications. By testing individual heater surfaces belonging to different species, insights regarding the different heating parameters have been provided. The insights might be useful in the design of devices for different applications such as wearable electronics, medical applications, and industrial fields. To design and further improve the efficacy and performance of heater surfaces, one can derive inspiration from the hierarchical surface topography of the leaves in combination with advanced fabrication technologies.

### Supporting Information

Supporting Information is available from the Wiley Online Library or from the author.

### Acknowledgements

This work was supported by the Academy of Finland (grants: #331368, #299087, #292477, and #326461) and KONE foundation. All authors are grateful for the support from the Tampere Microscopy Center for the characterization of the surfaces.

### Conflict of Interest

The authors declare no conflict of interest.

### Data Availability Statement

The data that support the findings of this study are available on request from the corresponding author. The data are not publicly available due to privacy or ethical restrictions.

### Keywords

Ag nanowires, bioinspiration, leaf skeletons, transparent heaters

Received: November 25, 2021

Revised: December 23, 2021

Published online:

- [1] R. Gupta, K. D. M. Rao, S. Kiruthika, G. U. Kulkarni, *ACS Appl. Mater. Interfaces* **2016**, *8*, 12559.
- [2] L. Veeramuthu, B.-Y. Chen, C.-Y. Tsai, F.-C. Liang, M. Venkatesan, D.-H. Jiang, C.-W. Chen, X. Cai, C.-C. Kuo, *RSC Adv.* **2019**, *9*, 35786.
- [3] D. T. Papanastasiou, A. Schultheiss, D. Muñoz-Rojas, C. Celle, A. Carella, J.-P. Simonato, D. Bellet, *Adv. Funct. Mater.* **2020**, *30*, 1910225.
- [4] M. N. Gueye, A. Carella, R. Demadrille, J.-P. Simonato, *ACS Appl. Mater. Interfaces* **2017**, *9*, 27250.
- [5] X. Chen, Y. Yin, W. Yuan, S. Nie, Y. Lin, W. Guo, W. Su, Y. Li, K. Yang, Z. Cui, *Adv. Electron. Mater.* **2021**, 2100611.
- [6] V. Sharma, A. Koivikko, K. Yiannacou, K. Lahtonen, V. Sariola, *NPJ Flex. Electron.* **2020**, *4*, 27.
- [7] S. Hong, H. Lee, J. Lee, J. Kwon, S. Han, Y. D. Suh, H. Cho, J. Shin, J. Yeo, S. H. Ko, *Adv. Mater.* **2015**, *27*, 4744.
- [8] B. Tian, Q. Liu, C. Luo, Y. Feng, W. Wu, *Adv. Electron. Mater.* **2020**, *6*, 1900922.
- [9] Q. Liu, B. Tian, J. Liang, W. Wu, *Mater. Horizons* **2021**, *8*, 1634.
- [10] Q. Liu, B. Tian, C. Luo, J. Liang, W. Wu, *Adv. Mater. Technol.* **2020**, *5*, 2000278.
- [11] L. Brosseau, K. A. Yonge, V. Welch, S. Marchand, M. Judd, G. A. Wells, P. Tugwell, *Cochrane Database Syst. Rev.* **2003**.
- [12] J. Jang, J.-W. Choi, *J. Mater. Chem. C* **2021**, *9*, 4670.
- [13] M. K. Roul, B. Obasogie, G. Kogo, J. R. Skuza, R. M. Mundle, A. K. Pradhan, *J. Appl. Phys.* **2017**, *122*, 135110.
- [14] J. C. Goak, T. Y. Kim, D. U. Kim, K. S. Chang, C. S. Lee, N. Lee, *Appl. Surf. Sci.* **2020**, *510*, 145445.
- [15] J. Kang, H. Kim, K. S. Kim, S.-K. Lee, S. Bae, J.-H. Ahn, Y.-J. Kim, J.-B. Choi, B. H. Hong, *Nano Lett.* **2011**, *11*, 5154.
- [16] O. Ergun, S. Coskun, Y. Yusufoglu, H. E. Unalan, *Nanotechnology* **2016**, *27*, 445708.
- [17] Y. Huang, Y. Tian, C. Hang, Y. Liu, S. Wang, M. Qi, H. Zhang, J. Zhao, *ACS Appl. Mater. Interfaces* **2019**, *11*, 21850.
- [18] Y. Zhu, Y. Deng, P. Yi, L. Peng, X. Lai, Z. Lin, *Adv. Mater. Technol.* **2019**, *4*, 1900413.
- [19] Y. J. Fan, X. Li, S. Y. Kuang, L. Zhang, Y. H. Chen, L. Liu, K. Zhang, S. W. Ma, F. Liang, T. Wu, *ACS Nano* **2018**, *12*, 9326.
- [20] Y. D. Suh, S. Hong, J. Lee, H. Lee, S. Jung, J. Kwon, H. Moon, P. Won, J. Shin, J. Yeo, S. H. Ko, *RSC Adv.* **2016**, *6*, 57434.
- [21] S. Han, S. Hong, J. Yeo, D. Kim, B. Kang, M.-Y. Yang, S. H. Ko, *Adv. Mater.* **2015**, *27*, 6397.
- [22] D. Kim, J. Kwon, J. Jung, K. Kim, H. Lee, J. Yeo, S. Hong, S. Han, S. H. Ko, *Small Methods* **2018**, *2*, 1800077.
- [23] S. Ding, Y. Tian, J. Jiu, K. Suganuma, *RSC Adv.* **2018**, *8*, 2109.
- [24] S. Han, J. Kim, Y. Lee, J. Bang, C. G. Kim, J. Choi, J. Min, I. Ha, Y. Yoon, C.-H. Yun, M. Cruz, B. J. Wiley, S. H. Ko, *Nano Lett.* **2021**, *22*, 524.
- [25] Y. Liu, W. Xiong, D. W. Li, Y. Lu, X. Huang, H. Liu, L. S. Fan, L. Jiang, J.-F. Silvain, Y. F. Lu, *Int. J. Extrem. Manuf.* **2019**, *1*, 25001.
- [26] Y.-R. Jang, W.-H. Chung, Y.-T. Hwang, H.-J. Hwang, S.-H. Kim, H.-S. Kim, *ACS Appl. Mater. Interfaces* **2018**, *10*, 24099.
- [27] D. P. Langley, M. Lagrange, G. Giusti, C. Jiménez, Y. Bréchet, N. D. Nguyen, D. Bellet, *Nanoscale* **2014**, *6*, 13535.
- [28] L. Xu, W.-C. Weng, Y.-C. Yeh, *Nanomater* **2021**, *11*, 2511.
- [29] J. Ha, B. J. Lee, D. J. Hwang, D. Kim, *RSC Adv.* **2016**, *6*, 86232.
- [30] P.-H. Wang, S.-P. Chen, C.-H. Su, Y.-C. Liao, *Rsc Adv.* **2015**, *5*, 98412.
- [31] L. Cai, A. Y. Song, P. Wu, P.-C. Hsu, Y. Peng, J. Chen, C. Liu, P. B. Catrysse, Y. Liu, A. Yang, *Nat. Commun.* **2017**, *8*, 1.
- [32] H. Park, P. Takmakov, H. Lee, *Sci. Rep.* **2018**, *8*, 4375.
- [33] L. V. Thekkekara, M. Gu, *Sci. Rep.* **2017**, *7*, 1.
- [34] Y. H. Sim, M. J. Yun, S. I. Cha, D. Y. Lee, *Proc. R. Soc. A* **2020**, *476*, 20200094.
- [35] S. James, R. Contractor, *Sci. Rep.* **2018**, *8*, 17032.
- [36] A. T. Bellew, H. G. Manning, C. Gomes da Rocha, M. S. Ferreira, J. J. Boland, *ACS Nano* **2015**, *9*, 11422.
- [37] D. A. Jones, D. A. Wilkins, in *Variation And Adaptation In Plant Species.*, Heine-Mann Educational Books Ltd., London, UK **1971**.
- [38] P. Won, J. J. Park, T. Lee, I. Ha, S. Han, M. Choi, J. Lee, S. Hong, K.-J. Cho, S. H. Ko, *Nano Lett.* **2019**, *19*, 6087.
- [39] A. Elsayes, V. Sharma, K. Yiannacou, A. Koivikko, A. Rasheed, V. Sariola, *Adv. Sustain. Syst.* **2020**, *4*, 2000056.
- [40] P. Li, Z. F. Zhang, *Sci. Rep.* **2017**, *7*, 4062.
- [41] A. Karperien, *Front. Cell. Neurosci.* **2013**, *7*, 3.
- [42] P. Shi, K. Yu, Ü. Niinemets, J. Gielis, *Forests* **2021**, *12*, 41.
- [43] J. E. de Araujo Mariath, R. P. dos Santos, *Rev. Bras. Biociências* **2010**, *8*, 30.
- [44] G. Haacke, *J. Appl. Phys.* **1976**, *47*, 4086.
- [45] Y. N. Zhou, *J. Mater. Chem.* **2012**, *22*, 12997.
- [46] S. Ji, W. He, K. Wang, Y. Ran, C. Ye, *Small* **2014**, *10*, 4951.
- [47] B. Han, Q. Peng, R. Li, Q. Rong, Y. Ding, E. M. Akinoglu, X. Wu, X. Wang, X. Lu, Q. Wang, *Nat. Commun.* **2016**, *7*, 1.